Large Tunneling Magnetoresistance in van der Waals Ferromagnet/Semiconductor Heterojunctions

*Wenkai Zhu, Hailong Lin, Faguang Yan, Ce Hu, Ziao Wang, Lixia Zhao, Yongcheng Deng, Zakhar R. Kudrynskyi, Tong Zhou, Zakhar D. Kovalyuk, Yuanhui Zheng, Amalia Patanè, Igor Žutić, Shushen Li, Houzhi Zheng, and Kaiyou Wang**

2D layered chalcogenide semiconductors have been proposed as a promising class of materials for low-dimensional electronic, optoelectronic, and spintronic devices. Here, all-2D van der Waals vertical spin-valve devices, that combine the 2D layered semiconductor InSe as a spacer with the 2D layered ferromagnetic metal Fe_3GeTe_2 as spin injection and detection electrodes, are reported. Two distinct transport behaviors are observed: tunneling and metallic, which are assigned to the formation of a pinhole-free tunnel barrier at the Fe_3GeTe_2/InSe interface and pinholes in the InSe spacer layer, respectively. For the tunneling device, a large magnetoresistance (MR) of 41% is obtained under an applied bias current of 0.1 µA at 10 K, which is about three times larger than that of the metallic device. Moreover, the tunneling device exhibits a lower operating bias current but a more sensitive bias current dependence than the metallic device. The MR and spin polarization of both the metallic and tunneling devices decrease with increasing temperature, which can be fitted well by Bloch's law. These findings reveal the critical role of pinholes in the MR of all-2D van der Waals ferromagnet/semiconductor heterojunction devices.

1. Introduction

2D van der Waals (vdW) layered non-magnetic materials, such as graphene and chalcogenide semiconductors, are promising candidates for spacer layers in spin-valve devices.[1–7] Perfect spin filtering and high magnetoresistance (MR) of ≈100% were predicted for Co/graphene/Co or Ni/graphene/Ni vertical spin valves with five or more graphene layers.[2,3] Subsequently, graphene-based spin-valve devices were extensively studied experimentally, but the measured MR was less than 5%.[8–14] Also, Fe/MoS_2/Fe spin-valve devices with a seven-layer MoS_2 spacer was predicted to present a maximum MR of ≈300%.[4] Another similar theoretical work has revealed that spin-valve devices with a single-layer MoS_2 spacer show a metallic behavior due to the strong coupling between MoS_2 and the ferromagnets.[5] In contrast, those with a few layer MoS_2 spacer are dominated by tunneling.[5] Experimental results show that in NiFe/MoS_2/Co vertical spin valves, the mono- to trilayer MoS_2 have metallic behavior, while the junctions with multilayer MoS_2 (≈8.1 nm) present tunneling mechanisms with a maximum MR of ≈3%, which is much smaller than that predicted theoretically.[15] In general, experiments on spin-valve devices based on other 2D materials, such as hBN, WS_2, WSe_2, BP, as the spacer layer, and on traditional ferromagnetic metals as the electrodes, also show only MR <6%.[16–19] The large discrepancy of MR between the theoretical and experimental results suggests that the measured MR is limited by the inevitable damage of the 2D

W. Zhu, H. Lin, F. Yan, C. Hu, Z. Wang, L. Zhao, Y. Deng, Y. Zheng, S. Li, H. Zheng, K. Wang
State Key Laboratory of Superlattices and Microstructures
Institute of Semiconductors
Chinese Academy of Sciences
Beijing 100083, China
E-mail: kywang@semi.ac.cn

W. Zhu, H. Lin, C. Hu, Z. Wang, Y. Deng, S. Li, H. Zheng, K. Wang
Center of Materials Science and Optoelectronics Engineering
University of Chinese Academy of Sciences
Beijing 100049, China

L. Zhao
Tiangong University
Tianjin 300387, China

The ORCID identification number(s) for the author(s) of this article can be found under https://doi.org/10.1002/adma.202104658.

DOI: 10.1002/adma.202104658

Z. R. Kudrynskyi, A. Patanè
School of Physics and Astronomy
University of Nottingham
Nottingham NG7 2RD, UK

T. Zhou, I. Žutić
Department of Physics
University at Buffalo
State University of New York
Buffalo, NY 14260, USA

Z. D. Kovalyuk
Frantsevich Institute for Problems of Materials Science
The National Academy of Sciences of Ukraine, Chernivtsi Branch
Chernivtsi 58001, Ukraine

Y. Zheng, K. Wang
Beijing Academy of Quantum Information Sciences
Beijing 100193, China

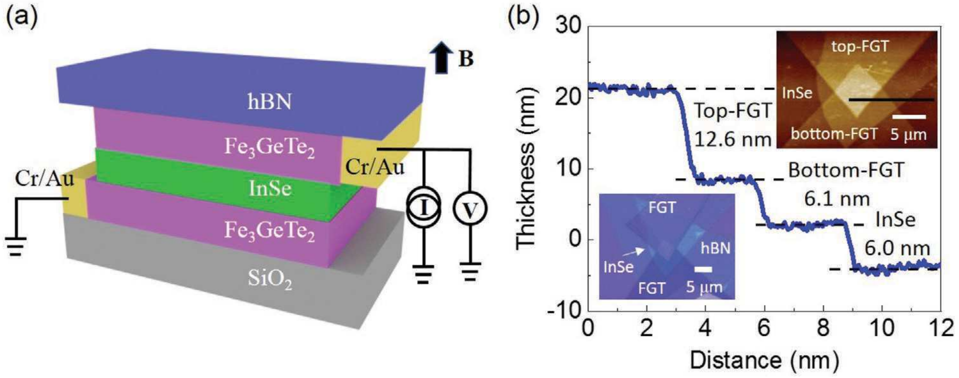

Figure 1. Device characterization. a) The schematic diagram of the device and magnetotransport setup. An out-of-plane magnetic field was applied to control the magnetization of the two FGT electrodes. b) AFM measurements of a typical device indicate that the thickness of the top FGT, bottom FGT, and spacer InSe are 12.6, 6.1, and 6.0 nm, respectively. The optical and AFM images of the device are shown in the bottom-left and upper-right corners, respectively (the scale bar is 5 μm).

materials interlayer and interface degradation occurring during the deposition of the 3D ferromagnetic layers.[20,21]

Recently, the 2D vdW intrinsic ferromagnetic metal Fe_3GeTe_2 (FGT) has attracted lots of attention because of its metallic nature, strong perpendicular magnetic anisotropy, and high Curie temperature (T_c) up to 220 K.[22–26] This allows researchers to build up all-2D vdW spin-valve devices with clean interfaces by mechanically exfoliation and dry transfer methods.[27] The FGT-based spin valves with a semiconductor or an insulator as the spacer layer, or even a ferroelectric layer have been proposed theoretically.[28–30] Experimentally, the tunneling FGT/hBN/FGT spin valves have been demonstrated and a high MR of 160% was achieved.[31] The semiconductor MoS_2 has also been used as the spacer layer in FGT/MoS_2/FGT devices, but the MoS_2 acts as a conductive layer rather than a tunneling barrier.[27] In addition, the FGT/FGT junctions shows a stable spin-valve effect even without any spacer layer.[32,33] However, except for the large MR (160%) for devices with an insulating hBN spacer layer, the MR for all-2D vdW spin valves with a semiconductor spacer is rather small (<5%). Hence, searching for more suitable spacer layers or device structures is highly desirable. Amongst 2D vdW crystals, indium selenide (InSe), is a metal chalcogenide semiconductor with unique electronic properties, including a sombrero-shaped valence band in few layers,[34] a thickness-dependent band structure (direct bandgap in the bulk and indirect bandgap in a few layers),[35] and high-electron mobility.[36] The choice of InSe and FGT is motivated by their close lattice match.[28] Furthermore, the FGT/InSe/FGT spin valve has been predicted to be a perfect spin-filter with a giant TMR ratio of up to 700%. This arises from the unique band structure of InSe, closely matched to that of FGT and large difference between the *k*-resolved transmission spectra in the parallel and antiparallel configurations.[28] However, so far, experimental work on the MR and conductive behavior of such spin-valve devices has not been reported.

In this work, we report on all-2D FGT/InSe/FGT vertical spin-valve devices. Devices with similar thickness of the spacer InSe show two distinct behaviors in the electrical transport: tunneling and metallic. The tunneling device shows nonlinear current-voltage characteristics and the resistance increases with decreasing temperature, which is attributed to the formation of a pinhole-free tunneling barrier between InSe and FGT. In contrast, the metallic device shows linear current–voltage characteristics and the resistance decreases with decreasing temperature from 230 to 130 K, which is assigned to the presence of pinholes in the InSe spacer layer. A large MR of up to 41% is achieved in the tunneling devices under applied currents below 0.1 μA at 10 K. The MR of the metallic devices is instead smaller (≈14%), which we assign to the existence of pinholes in the InSe layer. Overall, the MR of these structures is up to 50 and 10 times larger than the MR previously reported for NiFe/MoS_2/NiFe and FGT/MoS_2/FGT vertical spin valves, respectively. We examine the dependence of the MR on the bias current and temperature. The MR of the tunneling device is more sensitive to the bias current than the metallic one and can operate at lower bias currents. The MR ratio for both devices decrease with increasing temperature and the evolution of the spin polarization with temperature can be well fitted by Bloch's law.[37] Our results demonstrate a large MR in a 2D vdW ferromagnet/semiconductor heterojunction and the important role of pinholes in this type of spin-valve devices.

2. Results and Discussion

Figure 1a shows the schematic diagram of the FGT/InSe/FGT spin-valve structure, in which the layered semiconductor InSe is embedded between two ferromagnetic metal FGT electrodes and the junction area is covered with hBN to avoid contamination and oxidation in air. The cross-section high-resolution transmission electron microscopy image of the FGT/InSe heterostructure shows that the interface is atomically flat with the atomic layers in InSe and the FGT clearly visible (Figure S1, Supporting Information). This excludes a significant contamination of the layers/interface. The magnetotransport measurements were conducted with a magnetic field (B) applied perpendicular to the layer plane to control the magnetization direction of the two FGTs. As shown in Figure 1b, atomic force microscopy (AFM) measurements of a typical spin-valve device indicate that the thickness of the top FGT, bottom FGT, and spacer InSe layers are 12.6, 6.1, and 6.0 nm, respectively. The coercivity of the FGT depends not only on its geometry, but

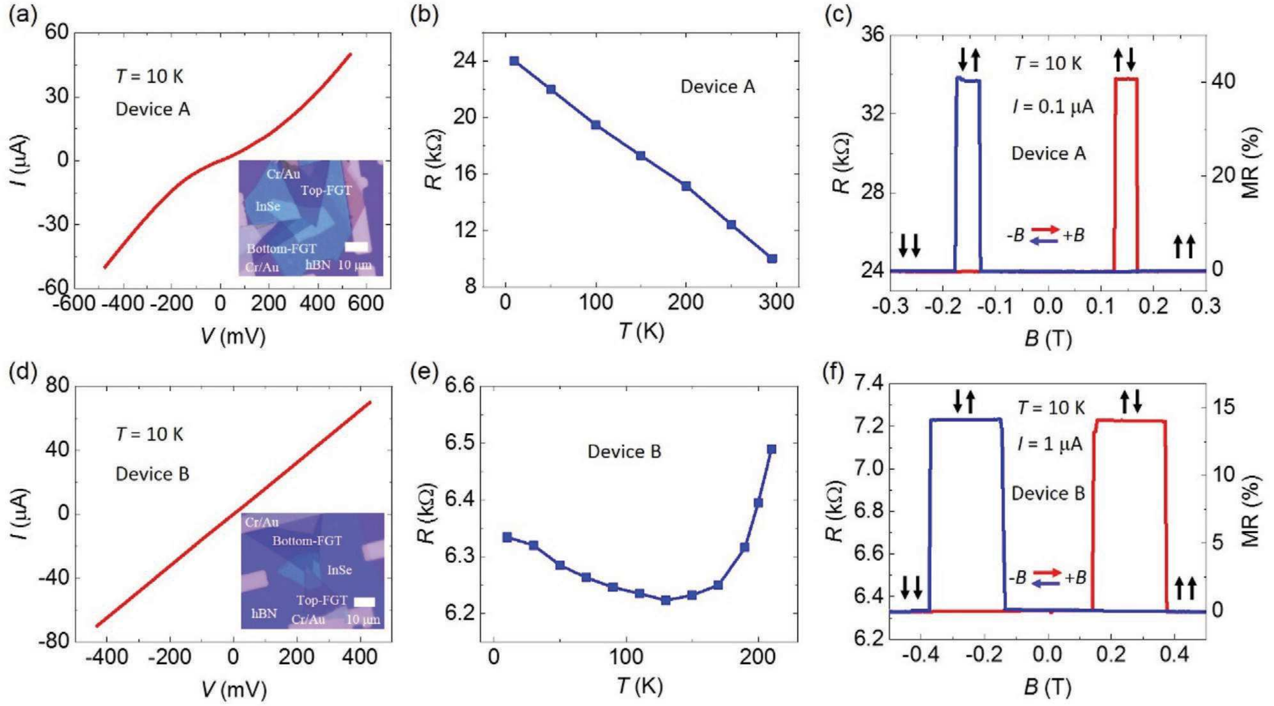

Figure 2. Electrical and magnetotransport properties of the FGT/InSe/FGT devices with tunneling (device A) or metallic (device B) behavior. a) *I–V* curve of device A at 10 K, showing nonlinear characteristics. Inset: optical image of device A. b) Resistance of device A as a function of temperature (*R–T*). c) Resistance as a function of the perpendicular magnetic field (*R–B*) of device A at a fixed current bias of 0.1 μA at 10 K. d) *I–V* curve of device B at 10 K, showing linear *I–V* characteristics. Inset: the optical image of device B. e) *R–T* curve of device B. f) *R–B* curve of device B measured at a fixed current of 1 μA at 10 K. The red and blue horizontal arrows show the sweeping directions of the magnetic field. The black vertical arrows denote the out-of-plane magnetization of the two FGTs.

also on the layer thickness.[26,38] Thus, in order to obtain very different coercivities between the top and bottom FGT electrodes, FGT flakes with different thickness were selected for fabricating the heterojunction. Photoluminescence and Raman studies show that the InSe spacer layer has a γ-rhombohedral phase with a bandgap energy of 1.39 eV at room temperature (Figure S2, Supporting Information), in good agreement with previous experimental results.[36] Also, anomalous Hall effect data of a typical exfoliated 15 nm-thick FGT show that the FGT is a 2D metallic ferromagnet with strong perpendicular magnetic anisotropy and relatively high T_c of 230 K (Figure S3, Supporting Information).

We have then investigated the electrical transport properties of two typical FGT/InSe/FGT devices (device A and B) by measuring the current–voltage (*I–V*) curves and the temperature evolution of the junction resistance (*R–T*). A relatively large magnetic field ($B = -0.4$ T) was applied before the *I–V* measurements to ensure that the two FGTs were in the parallel magnetic configuration. As shown in **Figure 2**a, the low temperature (10 K) *I–V* curve of device A is nonlinear, suggesting that a tunnel barrier is formed between InSe and the FGTs. The band alignment at the FGT/InSe interface from the theoretical calculations also reveals the existence of a tunnel barrier (Figure S4, Supporting Information).[28] The resistance decreases monotonically with rising the temperature, revealing a weak dependence in the measurement range from 10 to 295 K (Figure 2b), which suggests the device is a good tunnel junction with a pinhole-free barrier.[39] From the active overlap area of the device A (≈7.5 μm^2 from the optical microscopy image), we estimate a resistance–area product (*RA*) of 180 kΩ μm^2 at 10 K, which is comparable to the corresponding value in standard magnetic tunnel junctions.[31] However, we observed a distinct behavior in other devices with the same InSe layer thickness. For example, for device B in Figure 2d,e, the low temperature *I–V* curve is linear and with increasing the temperature from 10 to 230 K, the resistance first decreases and then increases, suggesting a metallic behavior.[27] The *RA* value of device B is estimated to be ≈45 kΩ μm^2 at 10 K. We note that although the two devices have the same layer thickness, the resistance of device A is almost four times larger than that of device B at 10 K. Thus, the hybridization between the ferromagnetic electrodes and the semiconductor spacer layer proposed before to explain the metallic behavior of spin valves cannot be used here to explain the very distinct transport behavior of our samples.[4,5,40] On the other hand, pinholes can affect the MR of magnetic tunnel junctions with a thin tunnel barrier. In the presence of pinholes, a percentage of electrons flow directly from the top to the bottom electrodes rather than tunneling throughout the barrier, thus decreasing the MR.[39,41,42] Pinholes can arise from the surface roughness of the tunnel barrier, whose thickness can be reduced in specific regions thus increasing the electron transmission.[42] Since our InSe flakes are atomically flat, this mechanism cannot explain our observations. On the other hand, pinholes can originate from point and/or line defects due to Se-vacancies and/or In-interstitials. Point defects can also coalesce to form extended line defects.[43] We have fabricated and investigated several devices with randomly different interlayer displacements and/or rotations occurring during the stacking process and these devices exhibit always two distinct transport behaviors with different *I*–*V* and *R*–*T* characteristics.

We examine now the MR of device A and B (Figure 2c,f). Upon sweeping the out-of-plane magnetic field *B* from negative to positive values, a sharp jump of the resistance from low to high-resistance state (R_{AP}) occurs. With further increasing *B*, the resistance jumps back to the low-resistance state (R_P). The symmetric resistance jumps are also observed for sweeping *B* from positive to negative values. The MR is derived from $(R_{AP} - R_P)/R_P$. For device A, this gives a MR value of 41%, which is about 50 and 10 times to that of the previous reported NiFe/MoS$_2$/NiFe and FGT/MoS$_2$/FGT vertical spin valves, respectively.[27,40] In contrast, the MR of device B is 14%, only 1/3 of that of device A. It proves that for the same thickness of the spacer layer, devices can have very different MR ratios. We attribute the reduced MR in device B to the existence of pinholes related to the defects in the InSe layer.[43,44] To further verify that the pinholes reduce the MR, we have fabricated several other devices with 6 nm-thick InSe, named devices C–E. The MR values and their dependence on the *RA* values for all our devices (A–B–C–D–E) are shown in Figure S5, Supporting Information. Devices with a lower *RA* values (<100 kΩ µm^2) show linear *I*–*V* characteristics and a smaller MR (≈1.6% in device C), while others with higher *RA* values exhibit nonlinear *I*–*V* characteristics and larger MR (≈54% in device E).

Since the operating current of a spin-valve device affects directly its performance, we studied the bias dependence of the MR for two of our spin-valve devices. As shown in **Figure 3**a, the tunneling device A exhibits perfect spin-valve signals at all bias currents (1 nA to 10 µA) and can work at low currents down to 1 nA at 10 K. The extracted bias-dependent MR ratios of device A is presented in Figure 3c. It can be seen that the ≈40% of MR ratios persists when the applied bias current is below 0.2 µA, indicating that the device can retain stable MR signals over a wide bias range. As the applied bias current exceeds 0.2 µA, the MR decreases approximately linearly as the bias current increases exponentially. We assign this dependence to scattering of higher energy electrons by localized trap states at the FGT/InSe interfaces.[45] In contrast, the device B shows perfect spin-valve signals in the measured bias range (10 nA to 70 µA) at 10 K (Figure 3b). It is worth noting that device B can only work at a minimum current of 10 nA. However, the maximum MR of 14% is obtained for device B, and the MR is not very sensitive to the bias current up to 2 µA (Figure 3d), which is ten times larger than that of device A. With further increasing the bias current, the device B shows the same downward trend as device A.[45] In addition, reversing the bias-current direction has very little influence on the magnitude of the MR ratios of device A and B, indicating the symmetrical interface in both vertical spin-valve devices (Figure S6a,b, Supporting Information). Finally we note that, for both devices A and B, the two

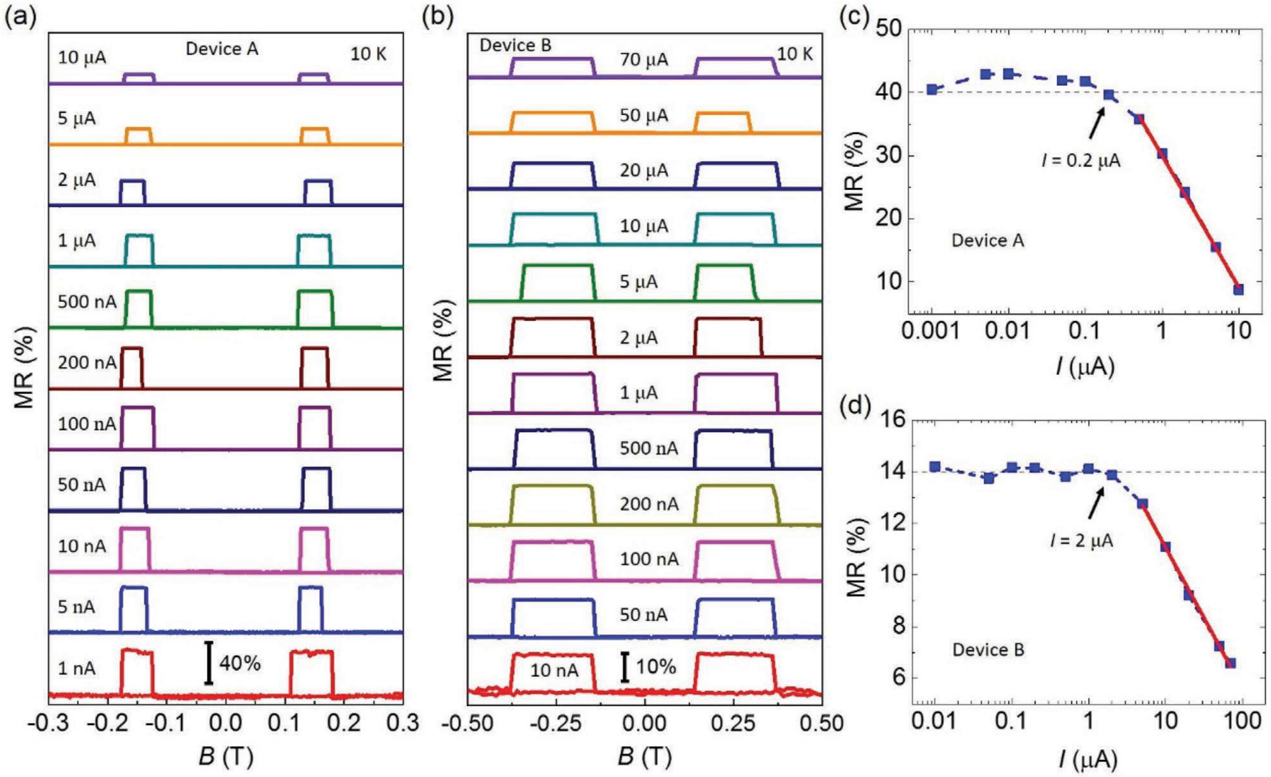

Figure 3. Bias-dependent spin-valve effect for device A and B. a) MR curves of device A at various bias currents ranging from 1 nA to 10 µA at 10 K. b) MR curves of device B at various bias currents ranging from 10 nA to 70 µA at 10 K. c) Extracted MR ratios of device A as a function of bias current. d) Extracted MR ratios of device B as a function of bias current.

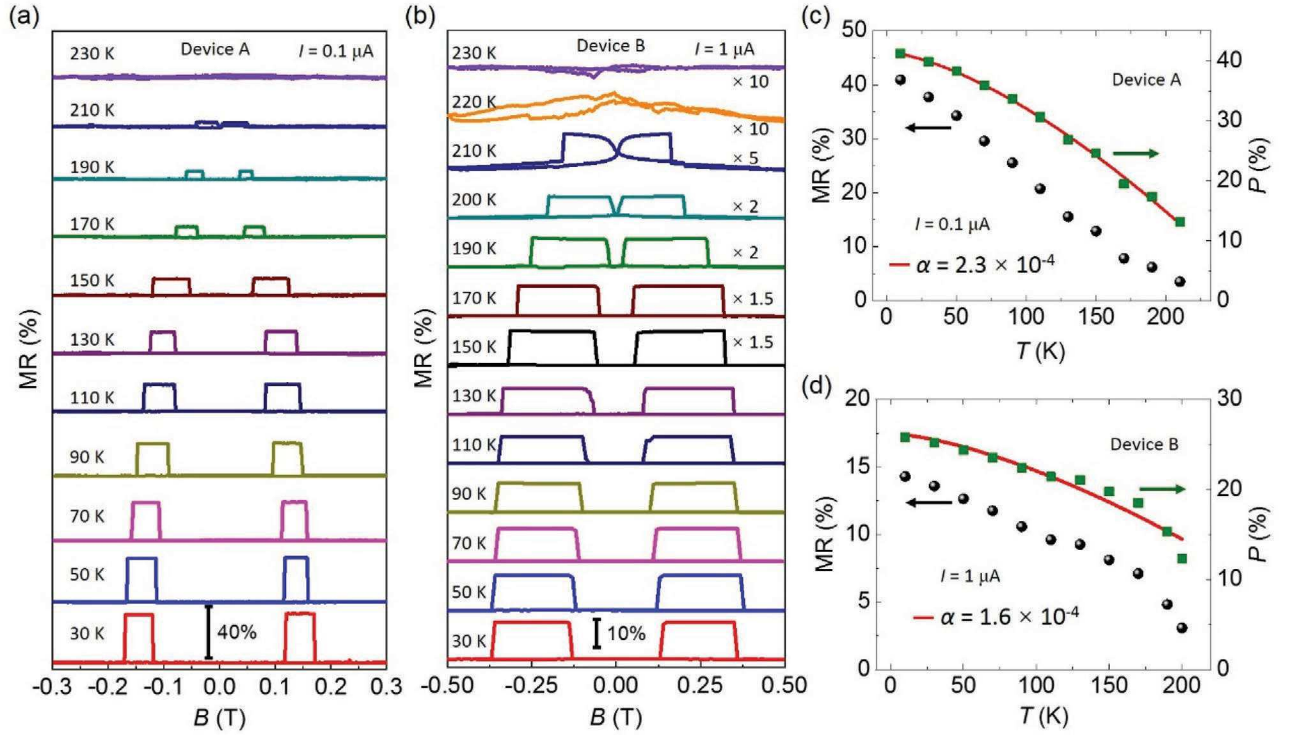

Figure 4. Temperature-dependent spin-valve effect for device A and device B. a) MR curves of device A measured at different temperatures in the range of 30–230 K with a constant bias current of 0.1 μA. b) MR curves of device B measured at different temperatures in the range of 30–230 K with a constant bias current of 1 μA. c) MR ratio and spin polarization of device A as a function of temperature. A fit to the data by Bloch's law (red line), give a material-dependent parameter $\alpha = 2.3 \times 10^{-4}$ K$^{-3/2}$. d) MR ratio and spin polarization of device B as a function of temperature. The red line shows the fit to the data by the Bloch's law, yielding a material-dependent parameter $\alpha = 1.6 \times 10^{-4}$ K$^{-3/2}$.

different resistance states measured in parallel and antiparallel magnetization configurations under zero magnetic field demonstrate the nonvolatile characteristic of the two different magnetic configurations (Figure S6c,d, Supporting Information).

In order to understand the temperature dependence of the MR in the spin-valve devices, MR curves of device A and B were measured at temperatures from 10 to 230 K. As shown in **Figure 4**a,b, the MR signals decrease monotonically with increasing the temperature and quench for $T > 210$ K, which corresponds to the T_c of the FGT. This phenomenon can be attributed to the decrease of spin polarization of the FGTs. The spin polarizations of both devices can be estimated using the Julliere model, which gives MR = $2P_1P_2/(1 - P_1P_2)$, where $P_{1(2)}$ denotes the spin polarization of the top (bottom) FGT electrode.[37,46] Here, we set $P_1 \approx P_2 = P$ due to the same nominal composition of the two FGT electrodes and symmetrical FGT/InSe interfaces. As shown in Figure 4c, the spin polarization P of the tunneling device A decreases from 41 to 13% as the temperature increases from 10 to 210 K. The maximum P is about three times larger than that obtained in other 2D semiconductor-based spin valves, such as graphene, MoS_2, or WS_2-based spin valves.[12,19,27] Similarly, the spin polarization P of the metallic device B decreases from 25.8 to 2.7% (Figure 4d). The estimated temperature dependence of the spin polarization can be fitted well by the Bloch's law, given by $P(T) = P_0(1 - \alpha T^{3/2})$, in which P_0 is the spin polarization at 0 K and α is a materials-dependent constant.[37,47,48] and the spin polarization decreases with increasing temperature due to spin-wave excitation.[48] The value of α is 2.3×10^{-4} K$^{-3/2}$ for the tunneling device A and 1.6×10^{-4} K$^{-3/2}$ for the metallic device B, which is similar to that observed in other FGT-based spin-valve devices.[27,31] The values of α in our devices is higher than those for Co (1–6 × 10^{-6} K$^{-3/2}$) and NiFe (3–5 × 10^{-5} K$^{-3/2}$), indicating a much stronger decay of spin polarization in our FGT-based devices as result of the lower Curie temperature of FGT.[48] This is also important in characterizing the spin injection in nonlocal spin-valve devices, where α may be further enhanced.[49]

3. Conclusions

We have fabricated all-2D FGT/InSe/FGT vertical spin-valve devices by a dry transfer method and investigated their magnetotransport properties. Devices with the same thickness of the spacer layer reveal tunneling and metallic behavior. A large MR of 41% is obtained for the tunneling device with applied currents below 0.1 μA at 10 K, which is about three times larger than that of the metallic device. The tunneling device exhibits a lower operating bias current, but more sensitive dependence on the bias current than the metallic device. Moreover, the MR ratios of both the metallic and tunneling devices decrease with increasing temperature, and the evolution of spin polarization with temperature can be fitted well by Bloch's law. The large MR in the tunneling device arises from a pinhole-free tunnel barrier between InSe and FGT. In contrast, the smaller MR in the metallic device is attributed to the existence of pinholes in the InSe layer. Our results prove that pinhole-free tunnel barriers in InSe-based all-2D vdW heterojunction devices can significantly enhance the MR and provide a desirable platform to integrate nonvolatile memory and spin logic.[7,50,51]

4. Experimental Section

Device Fabrication: For the FGT Hall bar, the four electrode regions were patterned on a 300 nm thick SiO_2/Si^{++} substrate by standard electron beam lithography, and Cr/Au (5/20 nm) electrodes were deposited on an ultrahigh vacuum evaporative sputtering system, followed by a lift-off process. Similarly, the Cr/Au (5/40 nm) electrodes for the two terminal FGT/InSe/FGT junctions were fabricated on a SiO_2/Si^{++} substrate prior to the transfer process using standard photoetching, evaporative sputtering and lift-off process. The high-quality vdW bulk single-crystals FGT and hBN were purchased from HQ Graphene, and InSe was grown by the Bridgman method at the Frantsevich Institute for Problems of Materials Science in Ukraine. First, a FGT flake was exfoliated onto poly(dimethylsiloxane) stamps by adhesive tape. The stamps were adhered to a glass slide. Under an optical microscope, the selected FGT flake with appropriate thickness and shape was transferred onto the pre-patterned 300 nm thick SiO_2/Si^{++} substrate by using a site-controllable dry transfer method.[27] Then, using the same method, an InSe flake was transferred onto the FGT flake, followed by another thicker FGT flake to form a FGT/InSe/FGT heterojunction device. The active overlap area of the device was ≈4–8 μm^2, which was smaller than the typical domain sizes in the FGT flakes.[52] In order to prevent the device from oxidation when exposed to air, a 20 nm-thick hBN layer was used to cap the whole heterojunction. Then, these devices were annealed at 120 °C for 10 min to ensure good adhesion between the layers and avoid the formation of bubbles. The exfoliation and stamping of the layers were performed and stored in a nitrogen-filled glovebox before loading into the low-temperature probe station.

Device Characterization: The electrical and magnetotransport studies were carried out in a Model CRX-VF Cryogenic Probe Station (Lake Shore Cryotronics) with a ±2.5 T out-of-plane vertical magnetic field over the temperature range from 10 to 500 K. The current–voltage curves were measured by a Keithley model 2602B SourceMeter and a Keithley model 2182A Nanovoltmeter. The thickness of the FGT and InSe flakes were determined by AFM (Bruker Multimode 8). Raman as well as photoluminescence spectra of InSe flakes were obtained by optical microscopy with excitation by a laser with wavelength of 532 nm (Renishaw inVia-Reflex). The cross-section transmission electron microscopy samples were prepared by using a focused ion beam (FEI Helios NanoLab 600i), and were characterized by using a FEI Tecnai G2 F20 microscope with an operating voltage of 200 kV.

Supporting Information

Supporting Information is available from the Wiley Online Library or from the author.

Acknowledgements

This work was financially supported by the National Key Research and Development Program of China (Grant Nos. 2017YFA0303400), the National Natural Science Foundation of China (Grant No. 61774144), the Key Research Program of Frontier Sciences (Grant Nos. QYZDY-SSW-JSC020), the Strategic Priority Research Program of Chinese Academy of Sciences (Grant Nos. XDB44000000 and XDB28000000). A.P. acknowledges the European Union's Horizon 2020 research and innovation programme Graphene Flagship Core 3. T.Z. and I.Ž. were supported by the US National Science Foundation ECCS-2130845.

Conflict of Interest

The authors declare no conflict of interest.

Data Availability Statement

The data that support the findings of this study are available from the corresponding author upon reasonable request.

Keywords

pinholes, tunneling magnetoresistance, van der Waals magnetism

Received: June 17, 2021
Revised: September 1, 2021

---

[1] T. M. G. Mohiuddin, E. Hill, D. Elias, A. Zhukov, K. Novoselov, A. Geim, *IEEE Trans. Magn.* **2008**, *44*, 2624.
[2] V. M. Karpan, G. Giovannetti, P. A. Khomyakov, M. Talanana, A. A. Starikov, M. Zwierzycki, J. van den Brink, G. Brocks, P. J. Kelly, *Phys. Rev. Lett.* **2007**, *99*, 176602.
[3] V. M. Karpan, P. A. Khomyakov, A. A. Starikov, G. Giovannetti, M. Zwierzycki, M. Talanana, G. Brocks, J. van den Brink, P. J. Kelly, *Phys. Rev. B* **2008**, *78*, 195419.
[4] K. Dolui, A. Narayan, I. Rungger, S. Sanvito, *Phys. Rev. B* **2014**, *90*, 041401.
[5] H. Zhang, M. Ye, Y. Wang, R. Quhe, Y. Pan, Y. Guo, Z. Song, J. Yang, W. Guo, J. Lu, *Phys. Chem. Chem. Phys.* **2016**, *18*, 16367.
[6] P. Lazić, K. D. Belashchenko, I. Žutić, *Phys. Rev. B* **2016**, *93*, 241401.
[7] H. Wen, H. Dery, W. Amamou, T. Zhu, Z. Lin, J. Shi, I. Žutić, I. Krivorotov, L. J. Sham, R. K. Kawakami, *Phys. Rev. Appl.* **2016**, *5*, 044003.
[8] M. Z. Iqbal, M. W. Iqbal, J. H. Lee, Y. S. Kim, S.-H. Chun, J. Eom, *Nano Res.* **2013**, *6*, 373.
[9] E. Cobas, A. L. Friedman, O. M. J. van't Erve, J. T. Robinson, B. T. Jonker, *Nano Lett.* **2012**, *12*, 3000.
[10] W. Li, L. Xue, H. D. Abruña, D. C. Ralph, *Phys. Rev. B* **2014**, *89*, 184418.
[11] J. Meng, J.-J. Chen, Y. Yan, D.-P. Yu, Z.-M. Liao, *Nanoscale* **2013**, *5*, 8894.
[12] J.-H. Park, H.-J. Lee, *Phys. Rev. B* **2014**, *89*, 165417.
[13] M. Z. Iqbal, G. Hussain, S. Siddique, M. W. Iqbal, *J. Magn. Magn. Mater.* **2017**, *429*, 330.
[14] P. U. Asshoff, J. L. Sambricio, A. P. Rooney, S. Slizovskiy, A. Mishchenko, A. M. Rakowski, E. W. Hill, A. K. Geim, S. J. Haigh, V. I. Fal'ko, I. J. Vera-Marun, I. V. Grigorieva, *2D Mater.* **2017**, *4*, 031004.
[15] M. F. Khan, H. Kim, G. Nazir, S. Jung, J. Eom, *Nanoscale* **2018**, *10*, 16703.
[16] M. Piquemal-Banci, R. Galceran, S. Caneva, M. B. Martin, R. S. Weatherup, P. R. Kidambi, K. Bouzehouane, S. Xavier, A. Anane, F. Petroff, A. Fert, J. Robertson, S. Hofmann, B. Dlubak, P. Seneor, *Appl. Phys. Lett.* **2016**, *108*, 102404.
[17] K. Zhao, Y. Xing, J. Han, J. Feng, W. Shi, B. Zhang, Z. Zeng, *J. Magn. Magn. Mater.* **2017**, *432*, 10.

[18] L. Xu, J. Feng, K. Zhao, W. Lv, X. Han, Z. Liu, X. Xu, H. Huang, Z. Zeng, *Adv. Condens. Matter Phys.* **2017**, *2017*, 9042823.

[19] V. Zatko, M. Galbiati, S. M.-M. Dubois, M. Och, P. Palczynski, C. Mattevi, P. Brus, O. Bezencenet, M.-B. Martin, B. Servet, J.-C. Charlier, F. Godel, A. Vecchiola, K. Bouzehouane, S. Collin, F. Petroff, B. Dlubak, P. Seneor, *ACS Nano* **2019**, *13*, 14468.

[20] M. Piquemal-Banci, R. Galceran, M.-B. Martin, F. Godel, A. Anane, F. Petroff, B. Dlubak, P. Seneor, *J. Phys. D: Appl. Phys.* **2017**, *50*, 203002.

[21] W. Zhang, P. K. J. Wong, X. Zhou, A. Rath, Z. Huang, H. Wang, S. A. Morton, J. Yuan, L. Zhang, R. Chua, S. Zeng, E. Liu, F. Xu, Ariando, D. H. C. Chua , Y. P. Feng, G. van der Laan, S. J. Pennycook, Y. Zhai, A. T. S. Wee, *ACS Nano* **2019**, *13*, 2253.

[22] H.-J. Deiseroth, K. Aleksandrov, C. Reiner, L. Kienle, R. K. Kremer, *Eur. J. Inorg. Chem.* **2006**, *2006*, 1561.

[23] C. Gong, X. Zhang, *Science* **2019**, *363*, eaav4450.

[24] S. Liu, X. Yuan, Y. Zou, Y. Sheng, C. Huang, E. Zhang, J. Ling, Y. Liu, W. Wang, C. Zhang, J. Zou, K. Wang, F. Xiu, *npj 2D Mater. Appl.* **2017**, *1*, 30.

[25] K. Kim, J. Seo, E. Lee, K. T. Ko, B. S. Kim, B. G. Jang, J. M. Ok, J. Lee, Y. J. Jo, W. Kang, J. H. Shim, C. Kim, H. W. Yeom, M. B. Il, B.-J. Yang, J. S. Kim, *Nat. Mater.* **2018**, *17*, 794.

[26] C. Tan, J. Lee, S.-G. Jung, T. Park, S. Albarakati, J. Partridge, M. R. Field, D. G. McCulloch, L. Wang, C. Lee, *Nat. Commun.* **2018**, *9*, 1554.

[27] H. Lin, F. Yan, C. Hu, Q. Lv, W. Zhu, Z. Wang, Z. Wei, K. Chang, K. Wang, *ACS Appl. Mater. Interfaces* **2020**, *12*, 43921.

[28] L. Zhang, T. Li, J. Li, Y. Jiang, J. Yuan, H. Li, *J. Phys. Chem. C* **2020**, *124*, 27429.

[29] X. Li, J.-T. Lü, J. Zhang, L. You, Y. Su, E. Y. Tsymbal, *Nano Lett.* **2019**, *19*, 5133.

[30] Y. Su, X. Li, M. Zhu, J. Zhang, L. You, E. Y. Tsymbal, *Nano Lett.* **2021**, *21*, 175.

[31] Z. Wang, D. Sapkota, T. Taniguchi, K. Watanabe, D. Mandrus, A. F. Morpurgo, *Nano Lett.* **2018**, *18*, 4303.

[32] C. Hu, D. Zhang, F. Yan, Y. Li, Q. Lv, W. Zhu, Z. Wei, K. Chang, K. Wang, *Sci. Bull.* **2020**, *65*, 1072.

[33] J. Kim, S. Son, M. J. Coak, I. Hwang, Y. Lee, K. Zhang, J.-G. Park, *J. Appl. Phys.* **2020**, *128*, 093901.

[34] V. Zólyomi, N. D. Drummond, V. I. Fal'ko, *Phys. Rev. B* **2014**, *89*, 205416.

[35] G. W. Mudd, M. R. Molas, X. Chen, V. Zólyomi, K. Nogajewski, Z. R. Kudrynskyi, Z. D. Kovalyuk, G. Yusa, O. Makarovsky, L. Eaves, M. Potemski, V. I. Fal'ko, A. Patanè, *Sci. Rep.* **2016**, *6*, 39619.

[36] D. A. Bandurin, A. V. Tyurnina, G. L. Yu, A. Mishchenko, V. Zólyomi, S. V. Morozov, R. K. Kumar, R. V. Gorbachev, Z. R. Kudrynskyi, S. Pezzini, Z. D. Kovalyuk, U. Zeitler, K. S. Novoselov, A. Patanè, L. Eaves, I. V. Grigorieva, V. I. Fal'ko, A. K. Geim, Y. Cao, *Nat. Nanotechnol.* **2017**, *12*, 223.

[37] I. Žutić, J. Fabian, S. D. Sarma, *Rev. Mod. Phys.* **2004**, *76*, 323.

[38] R. Skomski, H. P. Oepen, J. Kirschner, *Phys. Rev. B* **1998**, *58*, 3223.

[39] B. J. Jönsson-Åkerman, R. Escudero, C. Leighton, S. Kim, I. K. Schuller, D. A. Rabson, *Appl. Phys. Lett.* **2000**, *77*, 1870.

[40] W. Wang, A. Narayan, L. Tang, K. Dolui, Y. Liu, X. Yuan, Y. Jin, Y. Wu, I. Rungger, S. Sanvito, F. Xiu, *Nano Lett.* **2015**, *15*, 5261.

[41] Z. S. Zhang, D. A. Rabson, *J. Appl. Phys.* **2004**, *95*, 557.

[42] X. Chen, R. H. Victora, *Appl. Phys. Lett.* **2007**, *91*, 212104.

[43] D. G. Hopkinson, V. Zólyomi, A. P. Rooney, N. Clark, D. J. Terry, M. Hamer, D. J. Lewis, C. S. Allen, A. I. Kirkland, Y. Andreev, Z. Kudrynskyi, Z. Kovalyuk, A. Patanè, V. I. Fal'ko, R. Gorbachev, S. J. Haigh, *ACS Nano* **2019**, *13*, 5112.

[44] G. W. Mudd, A. Patanè, Z. R. Kudrynskyi, M. W. Fay, O. Makarovsky, L. Eaves, Z. D. Kovalyuk, V. Zólyomi, V. Falko, *Appl. Phys. Lett.* **2014**, *105*, 221909.

[45] J. Zhang, R. M. White, *J. Appl. Phys.* **1998**, *83*, 6512.

[46] M. Julliere, *Phys. Lett. A* **1975**, *54*, 225.

[47] J. Mathon, S. B. Ahmad, *Phys. Rev. B* **1988**, *37*, 660.

[48] C. H. Shang, J. Nowak, R. Jansen, J. S. Moodera, *Phys. Rev. B* **1998**, *58*, R2917.

[49] S. Garzon, I. Žutić, R. A. Webb, *Phys. Rev. Lett.* **2005**, *94*, 176601.

[50] H. Dery, H. Wu, B. Ciftcioglu, M. Huang, Y. Song, R. Kawakami, J. Shi, I. Krivorotov, I. Žutić, L. J. Sham, *IEEE Trans. Electron Devices* **2012**, *59*, 259.

[51] H. Dery, P. Dalal, Ł. Cywiński, L. J. Sham, *Nature* **2007**, *447*, 573.

[52] Z. Fei, B. Huang, P. Malinowski, W. Wang, T. Song, J. Sanchez, W. Yao, D. Xiao, X. Zhu, A. F. May, W. Wu, D. H. Cobden, J.-H. Chu, X. Xu, *Nat. Mater.* **2018**, *17*, 778.